# Molecular Dynamics Simulation, Free Energy Calculation and Structure-Based 3D-QSAR Studies of B-RAF Kinase Inhibitors

Ying Yang,[†] Jin Qin,[†] Huanxiang Liu,[‡] and Xiaojun Yao[†,§,*]

[†]State Key Laboratory of Applied Organic Chemistry and Department of Chemistry, Lanzhou University, Lanzhou 730000, China
[‡]School of Pharmacy, Lanzhou University, Lanzhou 730000, China
[§]Key Lab of Preclinical Study for New Drugs of Gansu Province, Lanzhou University, Lanzhou 730000, China

Ⓢ Supporting Information

ABSTRACT: ^{V600E}B-RAF kinase is the most frequent oncogenic protein kinase mutation in melanoma and is a promising target to treat malignant melanoma. In this work, a molecular modeling study combining QM-polarized ligand docking, molecular dynamics, free energy calculation, and three-dimensional quantitative structure—activity relationships (3D-QSAR) was performed on a series of pyridoimidazolone compounds as the inhibitors of ^{V600E}B-RAF kinase to understand the binding mode between the inhibitors and ^{V600E}B-RAF kinase and the structural requirement for the inhibiting activity. 3D-QSAR models, including CoMFA and CoMSIA, were developed from the conformations obtained by QM-polarized ligand docking strategy. The obtained models have a good predictive ability in both internal and external validation. Furthermore, molecular dynamics simulation and free energy calculations were employed to determine the detailed binding process and to compare the binding mode of the inhibitors with different activities. The binding free energies calculated by MM/PBSA gave a good correlation with the experimental biological activity. The decomposition of free energies by MM/GBSA indicates the van der Waals interaction is the major driving force for the interaction between the inhibitors and ^{V600E}B-RAF kinase. The hydrogen bond interactions between the inhibitors with Glu501 and Asp594 of the ^{V600E}B-RAF kinase help to stabilize the DFG-out conformation. The results from this study can provide some insights into the development of novel potent ^{V600E}B-RAF kinase inhibitors.
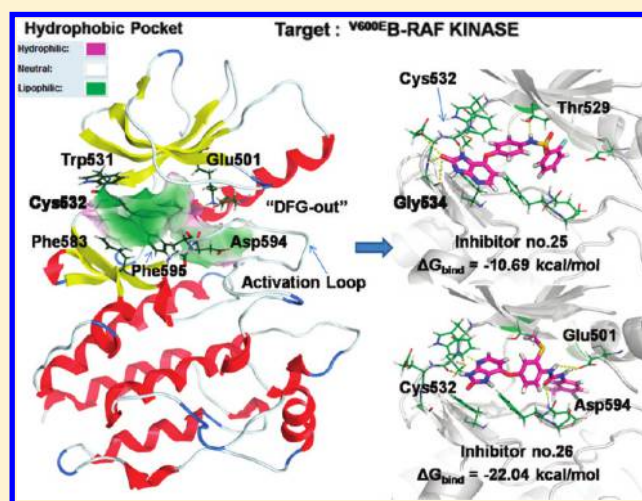
1. INTRODUCTION

RAF kinase plays a central role in the conserved RAS-RAF-MEK-ERK (MAPK) signal transduction pathway for cell proliferation and survival.[1] The RAF kinase family consists of three isoforms: A-, B-, and C-RAF. B-RAF is frequently mutated in a range of human cancers, most notably in melanoma (50—70%), thyroid (~30%), colorectal (~10%), and ovarian (~35%) cancers.[2,3] Over 500-fold elevated activity occurs in the most common mutation ^{V600E}B-RAF kinase (90%).[4,5] Therefore, B-RAF kinase and its mutations have emerged as important and exciting targets in cancer treatment.[6—8] In recent years, massive efforts have been made to develop B-RAF kinase inhibitors (well-known as PLX4032, RAF265, XL281, and Sorafenib).[9—13] Especially, the inhibitors targeting the highly frequent ^{V600E}B-RAF kinase mutation in melanoma are of great interest. The current B-RAF kinase inhibitors are mainly classified into two types: Type I occupies the ATP binding site in the active conformation of B-RAF kinase, and Type II recognizes the inactive conformation binding to another allosteric site adjacent to the ATP pocket.[13]

As an important technology and tool for drug design, computer-aided drug design methods have been applied to the discovery and design of B-RAF kinase inhibitors. For instance, Luo et al.[14] identified a series of selective purine-2,6-dione analogues as B-RAF kinase inhibitors using virtual screening technology. Fratev et al.[15—17] examined the molecular basis of the binding and selectivity of 26 pyrazine inhibitors by combined computational simulations and local-binding energy analysis. They also used molecular dynamics simulations to explain the effect of different inactivating mutations on the conformational stability of the protein. Alzate-Morales et al.[18] predicted the orientation of three pyrazole derivatives within B-RAF kinase
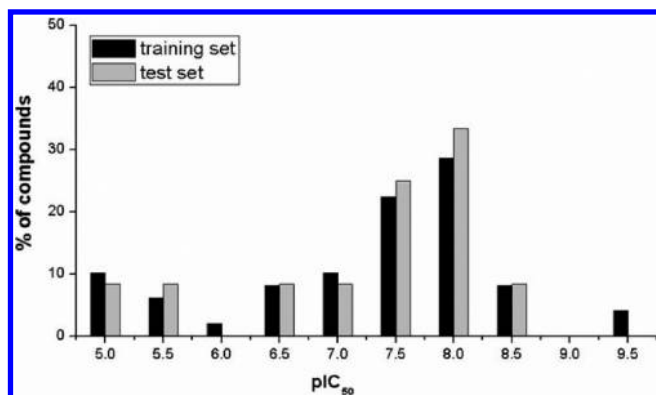
Figure 1. Distribution of the inhibiting activities for the training set and test set compounds in the 3D-QSAR study.

binding site using four docking methods and analyzed the interactions by molecular dynamics simulation.

Recently, Springer et al. reported a series of type II ^{V600E}B-RAF kinase inhibitors based on a tripartite A—B—C system.[19−24] With the pyridoimidazolone group as a new hinge-binding scaffold, the most active inhibitor notably achieves an IC_{50} of 1 nM with excellent *in vitro* potency both against the isolated enzyme and in mutant B-RAF driven cells. Because of the failure of Sorafenib with poor cellular activity against ^{V600E}B-RAF kinase in the treatment of malignant melanoma,[11] this improvement is considered a significant step for discovery of novel selective small molecule ^{V600E}B-RAF kinase inhibitors.

In the present study, we performed a molecular modeling study combining molecular docking, molecular dynamics (MD), molecular mechanics Poisson—Boltzmann surface area (MM/PBSA) calculations, and three-dimensional structure—activity relationship (3D-QSAR) analysis to investigate the detailed binding mode between ^{V600E}B-RAF kinase with this series of inhibitors and also to find the key structural features affecting the inhibiting activities. Considering the difficulty in the accurate estimation of electrostatic interaction, the QM-Polarized ligand docking and GBSA-rescoring were applied to predict probable poses of these inhibitors bound into the active site of ^{V600E}B-RAF kinase. To obtain the rational conformation for developing 3D-QSAR models, we applied the docking-based conformation selection strategy. Moreover, the detailed interactions were analyzed on the basis of the results from MD simulation and the free energy calculation for two inhibitors with much difference in their activity. The obtained results can help to understand the binding process and provide some insights into the further structural modification and development of new potent inhibitors.

2. METHODS AND COMPUTATIONAL DETAILS

Preparation of the Small Molecules. The 61 molecules together with their inhibiting activities were taken from the literature.[19,20] The 3D structures were sketched using Maestro[25] and geometrically minimized with Macromodel[26] based on OPLS-2001 force field. The structures and biological activities against ^{V600E}B-RAF kinase expressed as pIC_{50} are shown in Table S1 of the Supporting Information. The data set was divided into a training set for model generation and a test set for model validation, containing 49 and 12 compounds, respectively, for 3D-QSAR study. The test set compounds were selected by considering both the distribution of biological data and structural diversity (Figure 1).

In order to broaden the scope of the present 3D-QSAR investigation, we included an external test set of 23 compounds from that new series of compounds based on the tripartite "A—B—C" system (Table S4 of the Supporting Information) reported by the Springer group.[22−24] Selection of the external test set molecules was done on the basis of the structural diversity and wide range of biological activity similar to that of the training set.

Preparation of the Protein. The recently obtained crystal structure of ^{V600E}B-RAF kinase with high resolution was retrieved from the protein data bank (pdb code: 3IDP).[27] The missing loop region, which was not solved in the crystal structure, was modeled and refined in Discovery Studio 2.5.[28] The loop refinement method was employed to generate the rational atomic coordinates of missing loop. The energy-lowest and best-scored loop model was chosen as the initial structure among the top 10 randomized models. Furthermore, the structure was prepared in the following procedures by Maestro, including adding hydrogens, assigning partial charges using the OPLS-2001 force field and assigning protonation states, and structure minimizing in vacuum.[29] Finally, the cocrystal ligand was removed, and the resulting structure was used as the receptor model in the following studies.

QM-Polarized Ligand Docking (QPLD) and Molecular Mechanics-Generalized Born Surface Area (MM/GBSA)-Rescoring. After the structures were prepared, the popular docking program Glide and QM/MM software Q-site were combined to perform a QM-Polarized Ligand Docking (QPLD) study.[30] At first, a regular standard precision (SP) Glide docking following extra precision (XP) refinement was carried out, generating 10 poses per docked molecule, and then they were submitted to QM-ESP charge calculation at B3LYP/6-31G* level of theory within the protein environment defined by the OPLS-2001 force field. Finally, the resulting poses were redocked for another Glide run using the ESP atomic charges and XP scoring modes.

Furthermore, the docked poses were reranked in Prime.[31] The related postdocking scoring approach was the molecular mechanics-generalized Born surface area (MM/GBSA).[32,33] The protein structure was relaxed, and the energies were calculated using the OPLS-2001 force field and the GBSA continuum model on the basis of the flexible region within 22 Å (Huge) around the ligand, The docked poses were minimized using the local optimization strategy to calculate ligand binding energies. For each molecule, the best scoring pose was selected. The binding free energy ΔG_{bind} of ligand and protein was estimated as

$$\Delta G_{bind} = \Delta E_{MM} + \Delta G_{sol} - T\Delta S \qquad (1)$$

where, ΔE_{MM} is the difference in energy using the OPLS-2001 force field, ΔG_{sol} is the difference in the GBSA and nonpolar (estimated by the solvent accessible surface area) solvation energy, and $T\Delta S$ represents the entropy term. Corrections for entropic changes were not considered.

CoMFA and CoMSIA Analysis. 3D-QSAR models were developed in the program Sybyl6.9.[34] The alignment was achieved using the top-ranked docking pose (see above) for each inhibitor. By using the QPLD generated conformations, CoMFA[35] and CoMSIA[36] models were generated using the QSAR module with default parameters.[37,38] In the partial least-squares (PLS) regression analysis, a leave-one-out (LOO) cross-validation was first performed to find out the optimal number of components (ONC). Then further non-cross-validated analysis was done with ONC to obtain the final QSAR model.

Subsequently, bootstrapping analysis for 100 runs was performed to further assess the robustness and statistical confidence of the derived models.[39−42]

Molecular Dynamics Simulations. The MD simulations were performed in AMBER 10.0 software package[43] with the AMBER 03 force field.[44] The docked structures of [V600E]B-RAF kinase with compounds **25** and **26** were used as the initial structures for MD calculations. The force field parameters for the ligands were generated by the general AMBER force field (GAFF) using the Antechamber program.[45] The partial atomic charges for the ligand atoms were assigned using the RESP protocol[46] after electrostatic potential calculations at the B3LYP/6-31G* level. All hydrogen atoms of the protein were added using the leap module, considering ionizable residues set at their default protonation states at a neutral pH value. Each complex was neutralized by adding suitable counterions and solvated in a truncated octahedron box of TIP3P[47] water molecules with a margin distance of 10 Å. The particle mesh Ewald (PME) method was used for the long-range Coulombic interactions,[48] with a cutoff of 10.0 Å. The SHAKE algorithm[49] was employed on all atoms covalently bonded to hydrogen atoms, allowing for an integration time step of 2 fs. Periodic boundary conditions were applied to avoid edge effects in all calculations.

For equilibration, the solvent molecules and counterions, the side chain of protein, and the whole systems were successively minimized by 2500 steps of steepest descent method following 5000 steps of conjugated gradient method, while restraining the rest using a force constant of 500, 10, and 0 kcal/mol Å^2, respectively. Then each system was gradually heated from 0 to 300 K over a period of 50 ps and maintained at 300 K with a coupling coefficient of 1.0/ps with a force constant of 1.0 kcal/mol Å^2 on the complex. Each system was again equilibrated to a free simulation for 500 ps. Finally, a production run for 10 ns was performed using NPT ensemble at 300 K with 1.0 atm pressure. Coordinate trajectories were recorded every 1 ps for the whole MD runs.

Binding Free Energy Calculations. For each system, free energy calculations were performed for 400 snapshots extracted from the last 2 ns stable MD trajectory using AMBER10. For each snapshot, the free energy was calculated for each molecular species (complex, protein, and ligand), and the binding free energy is computed as the difference:

$$\Delta G_{bind} = G_{complex} - (G_{protein} + G_{ligand})$$
$$= \Delta G_{MM} + \Delta G_{sol} - T\Delta S \qquad (2)$$

The molecular mechanics energy was calculated by the electrostatic and van der Waals interactions:

$$\Delta G_{MM} = \Delta G_{ele} + \Delta G_{vdw} \qquad (3)$$

The solvation free energy was composed of the polar and the nonpolar contributions:

$$\Delta G_{sol} = \Delta G_{ele, sol} + \Delta G_{nonpol, sol} \qquad (4)$$

$\Delta G_{ele,sol}$ could be obtained by solving the Poisson−Boltzmann equation for MM/PBSA[50] method or the generalized Born equation for MM/GBSA method. Whereas the latter term $\Delta G_{nonpol,sol}$ was determined using

$$\Delta G_{nonpol, sol} = \gamma SASA + b \qquad (5)$$

where γ, representing the surface tension, and b, being a constant, were set to 0.0072 kcal/mol Å^2 and 0, respectively. SASA was the solvent accessible surface area (Å^2) determined using the linear combination of pairwise overlaps model.

The conformational entropy contributions (translation, rotation, and vibration) were estimated for 40 snapshots taken from the trajectories by using the Nmode module.[46] The structural minimizations and normal-mode analyses for the complex, protein, and ligand were carried out with a distance-dependent dielectric constant, $\varepsilon = 4r$, and convergence tolerance tighter than rmsd = 10^{-5} kcal mol^{-1} Å^{-1}.

Furthermore, the binding free energies were decomposed to a single residue using MM/GBSA method.[51−54] This decomposition was performed only for molecular mechanics and solvation energies but not for entropies.

3. RESULTS AND DISCUSSION

QPLD and GBSA-Rescoring. The QM-polarized docking was applied to predict the binding mode between [V600E]B-RAF kinase and its pyridoimidazolone inhibitors. This docking method can give a more accurate treatment of the electrostatic interactions, which help to improve the docking accuracy. First, the molecular docking method was validated by redocking the cocrystallized ligand from the binding site of [V600E]B-RAF. A lower rmsd of 0.15 Å and an XP score of −15.80 kcal/mol were finally obtained, compared with the regular Glide docking using the molecular mechanics method at the initial run of this QPLD protocol (rmsd = 0.82 Å, XP score = −12.05 kcal/mol). This demonstrated that the QPLD protocol reproduced well the experimentally observed binding mode for [V600E]B-RAF kinase inhibitor. Then all molecules were docked into the active site by the same way. Ten poses per molecule were submitted to the GBSA-rescoring process. The docking scores and GBSA-rescoring results versus activity for the top-ranking pose of each molecule are shown in Figure 2. The MM/GBSA scoring yields a little better correlation with the activities than that of the Glide XP function.

Figure 3a shows all 61 inhibitors docked into the binding pocket of [V600E]B-RAF kinase. All molecules were positioned in the same way, and most share a similar binding mode except for several molecules deviating from the hinge region of Cys532 due to low activity with unfavorable features for binding process. This might be associated with the relative rigidity of these molecules based on A-, B-, and C-ring segments for common scaffold.

The binding modes of the most active compound **26** and the least active compound **25** are shown in panels (c) and (b) of Figure 3, respectively. Accordingly, the pyridoimidazolone ring of compound **26** occupies the ATP binding pocket, interacting with three aromatic residues, Trp531, Phe583, and Phe595. It also forms hydrogen bonds between the pyridyl nitrogen and imidazolyl NH of **26** with the NH and C=O of Cys532 (NH−N, 2.017 Å, 153.9°) and (NH−O=C, 2.116 Å, 152.3°) of the hinge region. Besides, other important hydrogen bonds are observed between the urea group of **26** and the carboxylate side-chain of the conserved catalytic residue Glu501 (NH−O=C, 1.542 Å, 162.6°) and the main chain NH of Asp594 involved in the movement of the DFG loop (NH−O=C, 1.929 Å, 165.9°). Compared with the crystal structure of Sorafenib bound to inactive DFG-out conformational [V600E]B-RAF kinase (pdb code: 1UWJ), the compound **26** performs the same binding mode as Sorafenib with the inactive [V600E]B-RAF. This is also consistent with the docking study of compound **1** on the B-RAF/sorafenib cocrystal structure (pdb code: 1UWH) reported by the Springer group.[24] Furthermore, the docking of two new potent inhibitors **E1** and **E7** in the external test set shows the similar binding mode
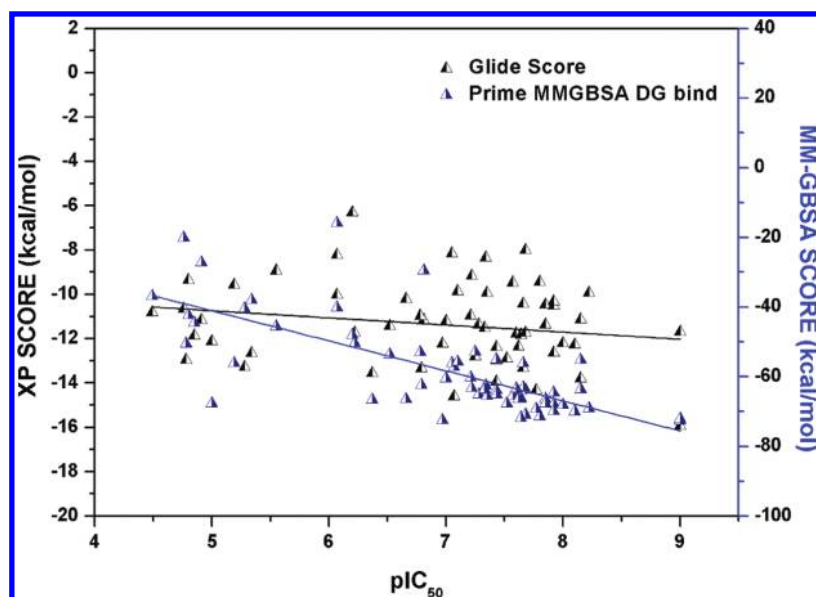
Figure 2. Docking scores and GBSA scores versus pIC_{50}.

with that of compound **26** (Figure S2 on the Supporting Information). Whereas compound **25** flips down the pyridoimi-dazolone ring to form hydrogen bonds between the imidazolyl NH and the C=O of Cys532 (NH—O=C, 2.348 Å, 142.1°) and C=O with NH of Gly 534 (NH—O=C, 1.609 Å, 159.3°) in the hinge region. The −NH of the sulfanilic amide linker in compound **25** forms an additional hydrogen bond with the hydroxyl side-chain of Thr529 (NH—OH, 1.923 Å, 169.6°). Comparing compound **25** with compound **26**, the H-bond interaction mode has changed in the hinge region, and the key bridging H-bond network between Glu501 and Asp594 could not be formed to stabilize the DFG-out conformation for ^{V600E}B-RAF kinase. This difference in the binding modes results in the distinct activities. The detailed interactions will be discussed further in the following investigations.

CoMFA and CoMSIA Statistical Results. As a comparison, we also developed the models on the basis of atom-fit alignment. The details are provided in the Supporting Information. The statistical parameters are summarized in Table 1. As shown in Table 1, the docking-based 3D-QSAR models have a better statistical result. Therefore, we focus on the DBA models in the following discussion. In the DBA models, the cross-validated PLS statistics of CoMFA and CoMSIA for the training set yields a correlation coefficient q^2 of 0.663 with ONC of 6 and 0.764 with 6, respectively. The noncross-validated PLS regressions sequentially give a coefficient r^2 of 0.961 with standard error of estimate (SEE) of 0.242 and 0.962 with 0.237, respectively. The boot-strapped results have r^2_{boot} of 0.976 ± 0.009, 0.980 ± 0.004, and SEE_{boot} of 0.184 ± 0.106 and 0.171 ± 0.077 for CoMFA and CoMSIA, respectively, suggesting that a good internal consistency exists within the training data set.

In the built CoMFA model, the steric field contribution is nearly twice that of the electrostatic contribution. In the CoMSIA model, the hydrophobic and H-acceptor and H-donor contributions share the large part. In our docking study, it was also recognized that the hydrophobic effect and H-bond network around the key residues of the active site plays a significant role in the binding. It also proves that the hydrophobic properties are important in the design of Type II ^{V600E}B-RAF kinase inhibitors.

Validation of CoMFA and CoMSIA Models. Both the test set with 12 compounds and the external test set with 23 compounds were used to validate the reliabilities of the built models. The predicted r^2_{pred} values for the test set from CoMFA and CoMSIA were 0.823 and 0.893, respectively. For the external test set, the corresponding r^2_{pred} values were 0.866 and 0.801 from CoMFA and CoMSIA, respectively, indicating our models have good predictive ability. The experimental and predicted pIC_{50} values for the training set, the test set, and the external test set are listed in Tables S2 and S5 of the Supporting Information, and the correlation plots are shown in Figure 4 and Figure S3 of the Supporting Information.

Interpretation of Structure-Based CoMFA and CoMSIA Contour Maps. In order to further explore the structure−activity relationship of these ^{V600E}B-RAF kinase inhibitors, the steric and electrostatic contour maps of the structure-based CoMFA and CoMSIA models are shown in Figure 5 and panel (a) of Figure 6. The hydrophobic, H-bond donor, and H-bond acceptor contour maps of CoMSIA are shown in panels (b) and (c) of Figure 6. The most active compound **26** is used for further analysis. Key residues in the active site are displayed in the figures.

In the CoMFA steric contour (Figure 5a), the green regions represent that the introduction of bulky groups may increase activity, while it is steric-unfavorable that bulky groups stretch toward the direction of yellow regions. It has been recognized that the 3-position of the B-ring is encompassed by a green contour. According to the binding site, the B-ring group interacts with the aromatic residue Phe595 of DFG motif in the allosteric site. It can be reasonably assumed that the B-ring core with a bulky substituent could provide a strong interaction to stabilize the inactive conformation of ^{V600E}B-RAF kinase. This region is also found in the contour map of CoMSIA. This observation is consistent with the experimental activity that compound **35** with a phenyl ring here is far less active than that with other substituents (**26**-SMe, **29**-F, and **37**-Cl). The two green contours covering the 2- and 5-positions of the C-ring, accompanied by the appearance of yellow contours, indicate that these positions should be occupied by the steric moderate and less crowded
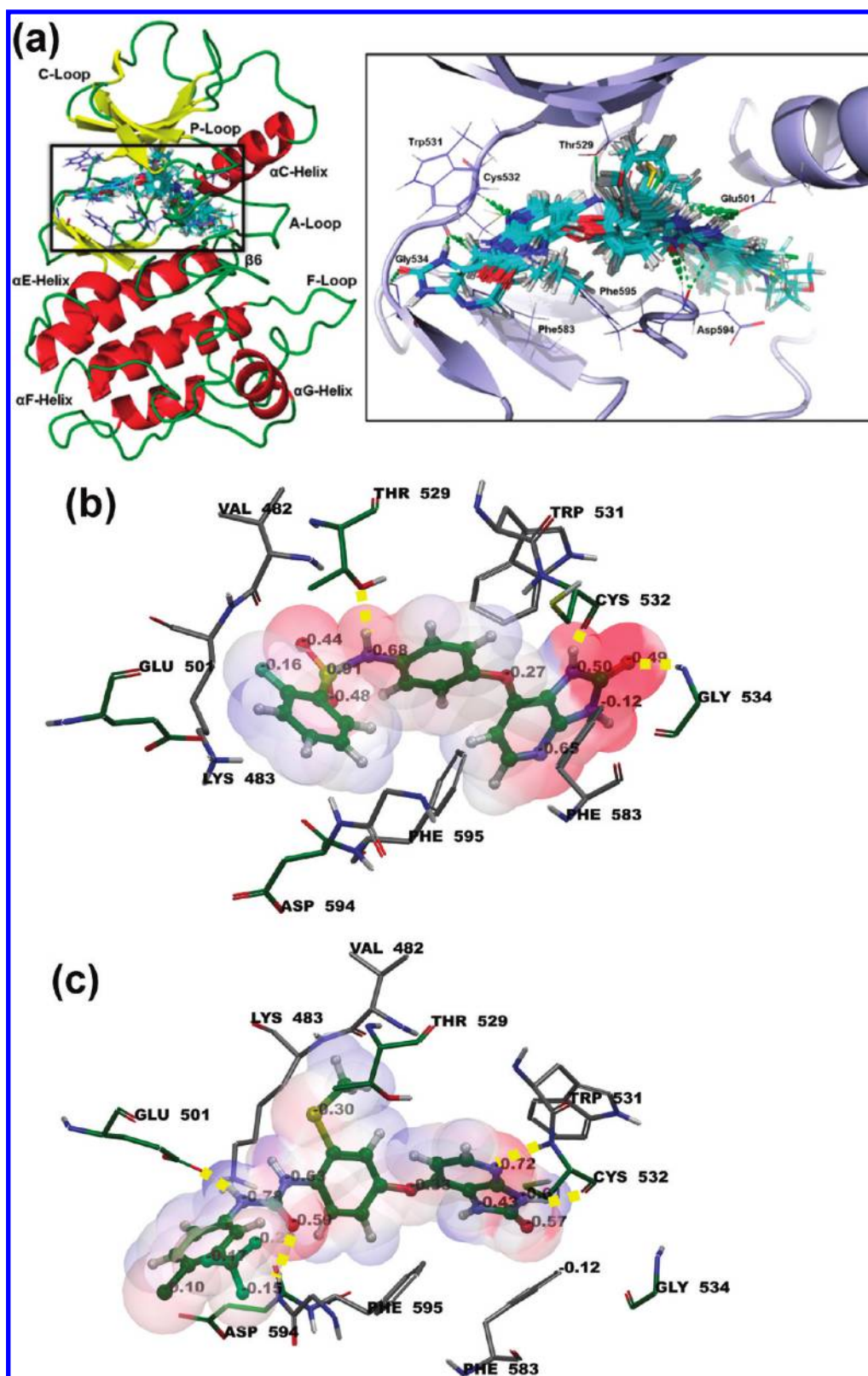
Figure 3. Binding mode between ^{V600E}B-RAF kinase and its inhibitors: (a) all 61 compounds, (b) compound **25**, and (c) compound **26** at the active site. Electrostatic potential surfaces are generated for compounds **25** and **26**, with heavy atom charges labeled.

substituents. The green contour near the group $-CF_3$ of the 3-position C-ring suggests bulky substituents may increase activity. This observation reflects the varying trend of activity for compounds **1**−**18**. Especially, 200-fold improvement in IC_{50}

for ^{V600E}B-RAF kinase is achieved for compound **3** ($-CF$) compared to compound **8** (-F). The small yellow contour near the 4-position of C-ring indicates the ortho-position steric hindrance effect.

On the CoMFA electrostatic contour map (Figure 5b), the blue regions indicate that the electropositive groups are favorable, and the red regions are contrary. It is shown that the blue region appears around N1 of the A-ring. Whereas, there are both blue and red contours around the linker between the A-ring and B-ring, which suggests electrostatic contributions have little effect on the activity. The blue region around the phenyl urea group shows key positive-favorable property, which reflects an important H-bond donor feature of both NH, here consistent with the docking study. This also is consistent with the experimental findings as the replacement of NH with the phenyl ring results in decreasing activity of compounds 19—22, 24, 60, and 61. The large blue region located on the 2- and 4-positions of the C-ring represents that the electropositive

groups are favorable for enhancing activity. The large red contour above the 3-position of the C-ring demonstrates that the negative-favorable substituents induce the positive carbon of phenyl ring.

The CoMSIA steric and electrostatic contours (Figure 6a) were found to be nearly identical to the corresponding CoMFA contours except for several slight differences. Because these contours were discussed above in the CoMFA model, so the following analyses focus on the CoMSIA H-bond donor and acceptor contours as well as the hydrophobic contours (in Figure 6b, c).

In the contour maps of the hydrophobic field, the white region is hydrophilic-favorable, while the yellow region is hydrophobic-favorable. As panel (b) of Figure 6 indicates, two white regions are in proximity to the polar urea group and 1- and 4-positions of the C-ring regions, which interact with polar and hydrophilic amino acid residues, such as Glu501, Thr508, and Asp594. The yellow regions are situated close to the 3-position of the C-ring and the 3-position of the B-ring. It is shown that both positions are pointing toward the hydrophobic pocket of the binding site, interacting with the Ile513, His574, Ile572 regions and the Val482, Ile527, Val528 regions, respectively. The groups at both positions should fit into the hydrophobic binding site to enhance the bioactivity. This is consistent with the CoMFA steric contour map, in which the sterically more bulky substituent is preferred for an increase in inhibitory activity.

The CoMSIA H-bond donor and acceptor contour map correlates with the involvement of H-bond interactions with the target. As shown in panel (c) of Figure 6, there are cyan donor-favorable and red acceptor-unfavorable contours over the NH of the urea group and the imidazolyl NH of the A-ring. Whereas a prominent purple donor-unfavorable contour occurs right close to the magenta acceptor-favorable regions oriented by the pyridyl nitrogen of the A-ring and the C═O of the urea group.

From the above, we can conclude:

(i) Pyridylimidazolyl of the A-ring and urea group between B- and C-rings should have a key H-bond acceptor and donor.

(ii) The 3-position substituent of the B-ring should be hydrobolic bulky to interact with the DFG motif toward the allosteric site.

Table 1. Summary of the Results for CoMFA and CoMSIA Models[a]

	CoMFA		CoMSIA	
PLS	ABA	DBA	ABA	DBA
q^2	0.613	0.663	0.729	0.764
ONC	4	6	5	6
r^2	0.916	0.961	0.940	0.962
SEE	0.346	0.242	0.295	0.237
F_{test}	119.800	170.420	134.642	177.611
q^2_{boot}	0.939 ± 0.020	0.976 ± 0.009	0.962 ± 0.012	0.980 ± 0.004
SEE_{boot}	0.286 ± 0.165	0.184 ± 0.106	0.229 ± 0.113	0.171 ± 0.077
$r^2_{pred}{}^b$	0.746	0.823	0.809	0.893
$r^2_{pred}{}^c$	0.840	0.866	0.629	0.801
Field				
S	0.712	0.612	0.096	0.082
E	0.288	0.388	0.158	0.183
H	—	—	0.264	0.265
D	—	—	0.207	0.273
A	—	—	0.275	0.197

[a] Abbreviations: ABA (atom fit-based alignment), DBA (docking-based alignment), S (steric); E (electrostatic), H (hydrophobic), D (H-bond donor), A (H-bond acceptor). [b] For the test set. [c] For the external test set.
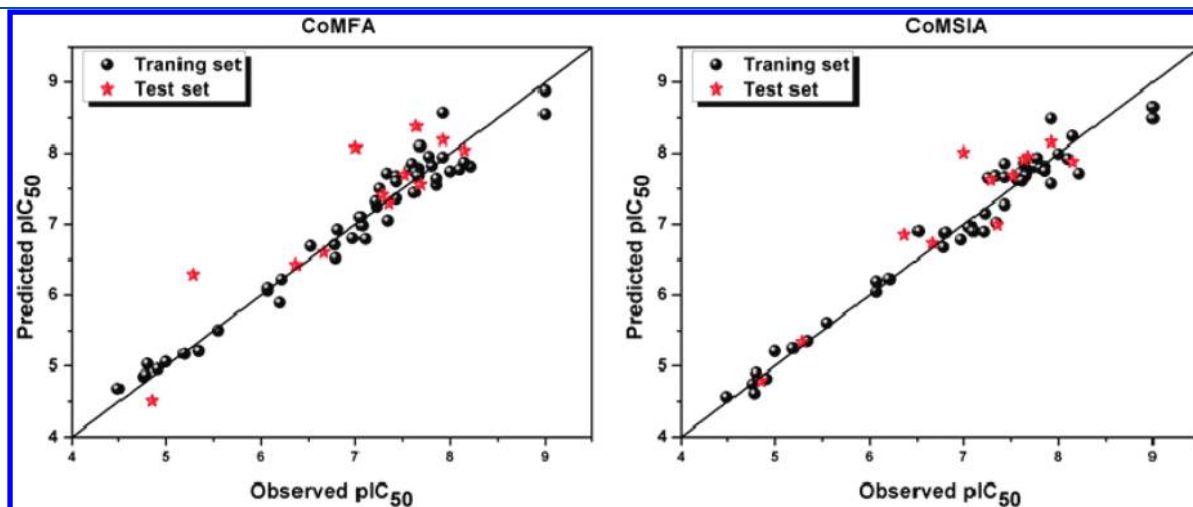

Figure 4. Plots of the predicted versus observed pIC_{50} values for 3D-QSAR models.
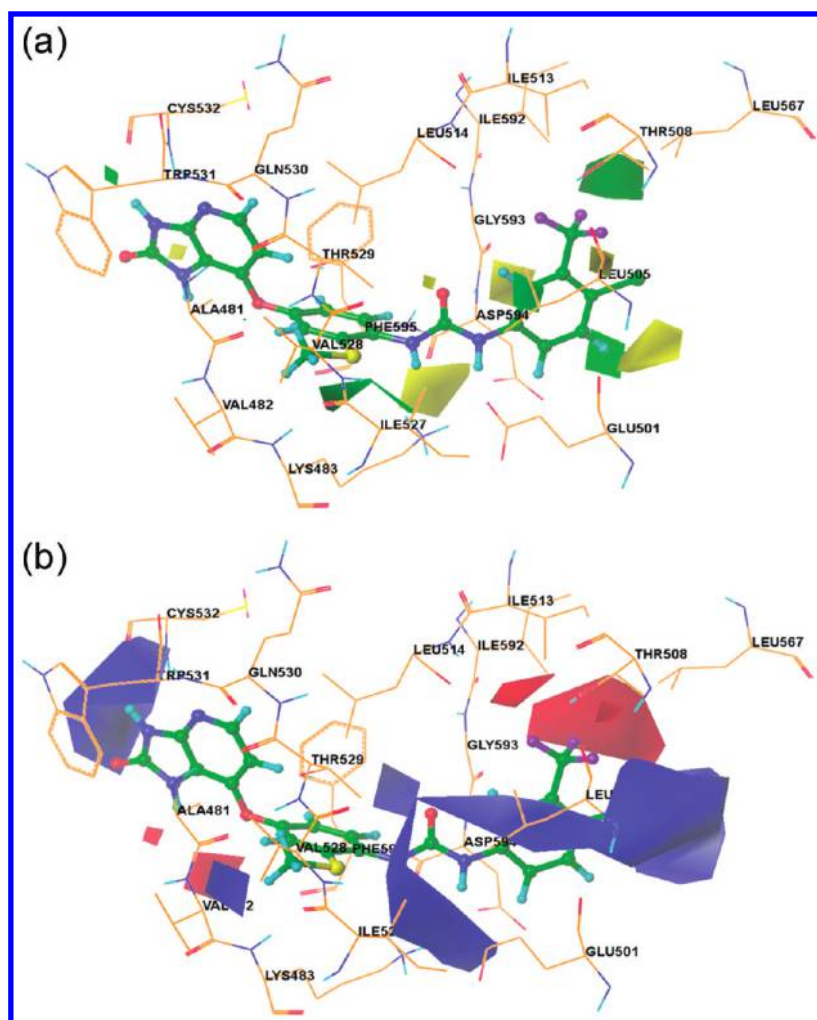
Figure 5. CoMFA StDev*Coeff contour maps based on the most active compound **26**. (a) Steric fields: favored (green) and disfavored (yellow). (b) Electrostatic fields: electropositive (blue) and electronegative (red).

(iii) The C-ring provides more modifiable information: 2- and 5-positions should be steric unfavorable; the 3-position is in favor of hydrophobic, negative, and bulky groups; the 4-position could be positive; and the 6-position is hydrophilic-favorable.

Molecular Dynamics Simulations of Compounds 25- and 26-Bound ^{V600E}B-RAF Kinase Systems. In order to compare the differences between the most active and the least active inhibitors in the binding process, molecular dynamics simulations for compounds **25**- and **26**- (**d25** and **d26**) bound ^{V600E}B-RAF kinase in explicit aqueous solution were run for 10 ns. To explore the dynamic stability of both systems and to ensure the rationality of the sampling method, root-mean-square deviations (rmsd) from the starting structure are analyzed (Figure 7a, b). The plots show that both studied systems reach equilibrium within 4 ns. The protein and ligand in the **d26**-bound system are stable after equilibrium, with average 1.3 Å and 0.8 Å rmsd fluctuation, respectively, while the corresponding values for the rmsd for the **d25**-bound system are significantly larger with longer time to equilibrium.

Furthermore, analyses of root-mean-square fluctuation (RMSF) versus the residue number for both systems are illustrated in panel (c) of Figure 7. The protein structures of the two systems share similar RMSF distributions and similar trends of dynamic features. It shows that there are four major flexible protein segments corresponding to the C-loop (residues 492−506), the F-loop between the A-loop and the αF-helix (residues 625−634), the A-loop (residues 593−623), and the αG-helix (residues 660−672) (Figure 3a). The fluctuations of the residues are higher in the **d25**-bound system than that in the **d26**-bound system. The fluctuations of the residues in the A-loop region around the allosteric site (593−602) are larger in the **d25**-bound system than that in the **d26**-bound system. The active site, including Glu501, Leu505, Thr508, Ile527−Cys532, and Asp594−Phe595, has larger conformational drift for the **d25**-bound system than that for the **d26**-bound system. Overall, these analyses for binding stabilization consist with the experimental activities.

The important hydrogen bond interactions from MD are listed in Table 2. A hydrogen bond is defined by distance (<3.5 Å) and orientation (the angle A···H-D >120.0°). It is shown that Glu501, Cys532, and Asp594 solidly form four hydrogen bonds with compound **26** from the initial structure to the end of simulation, while compound **25** forms one stable H-bond with Cys532 and another relatively weak H-bond with Gly534, accompanied by one occasionally formed hydrogen bond with Thr529. Besides, in both systems, water molecules mediate a hydrogen-bonding network among residues and ligands. In the
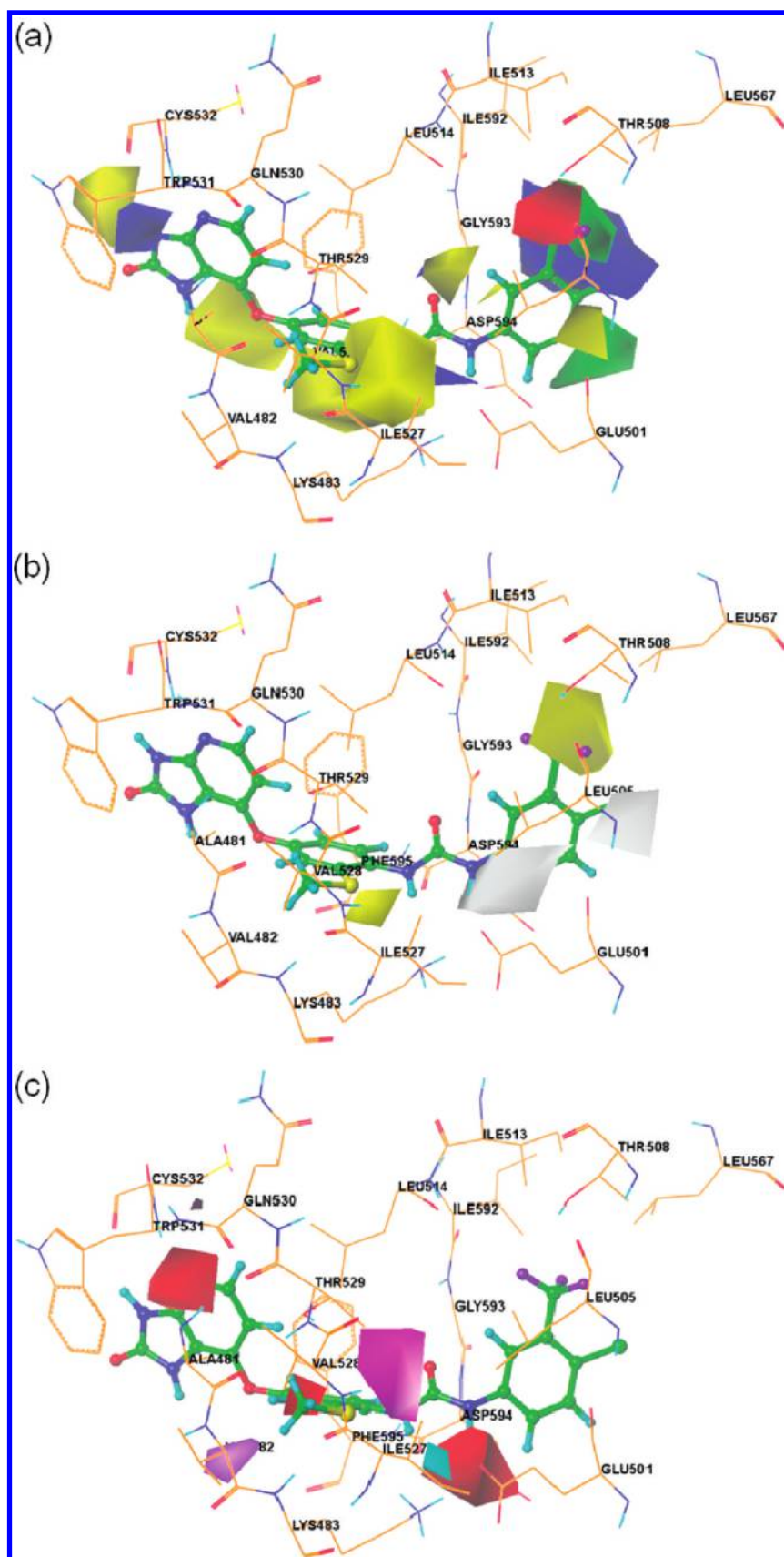
686

dx.doi.org/10.1021/ci100427j |*J. Chem. Inf. Model.* 2011, 51, 680–692

Figure 6. CoMSIA StDev*Coeff contour maps based on the most active compound **26**. (a) Steric and electrostatic fields (same as CoMFA). (b) Hydrophobic field: favored (yellow) and disfavored (white). (c) Hydrogen bond donor field: favored (cyan) and disfavored (purple). Hydrogen bond acceptor field: favored (magenta) and disfavored (red).
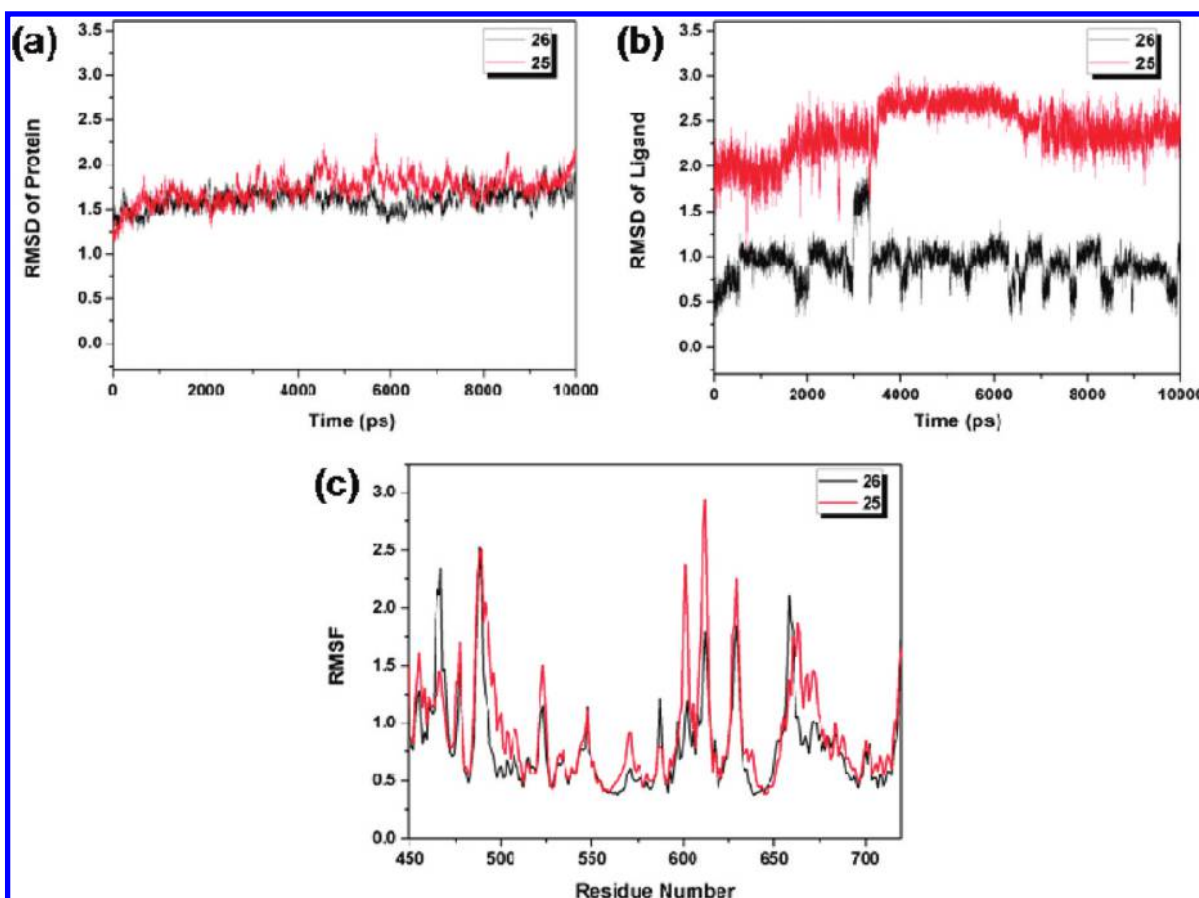
Figure 7. The rmsd of backbone atoms (C, Cα, and N) of the protein (a) and the heavy atoms in the ligand (b) for the **d25**-bound and **d26**-bound [V600E]B-RAF kinase systems as a function of the simulation time. (c) RMSF of the protein Cα atom for each residue for the **d25**-bound and **d26**-bound [V600E]B-RAF kinase systems.

d26-bound system, one water forms a H-bond with the ligand for stabilizing the interaction. The average structure of this water molecule can be observed in Figure 8. Whereas in the **d25-bound** system, the primary H-bond interactions with Glu501 and Asp594 cannot be formed with the compound **25** and are finally solvated by bulk water molecules in the trajectory.

Binding Free Energy Analysis. The binding affinities of both compounds with [V600E]B-RAF kinase were calculated using the MM/PBSA method. The results are shown in Table 3. It can be seen that there is a large difference of the calculated binding free energy for compounds **25** and **26**, which corresponds to the difference in the binding affinity. The IC_{50} value of compound **25** is about 32500 times higher than that of compound **26**. The $\Delta G_{bind,exp}$ is estimated to be 6.19 kcal/mol difference for compounds **25** and **26** approximately from IC_{50} values via $\Delta G \approx -RT \ln IC_{50}$.[55] Consequently, the calculated binding free energies are greatly compatible with the experimental ones. Although the calculated binding free energy is lower than that derived from the experiment because of the low prediction accuracy of entropic calculation and the approximation of experimental free energy, it is still of significance to compare their relative magnitude.

According to the energy individual components of the binding free energies (Table 3), the van der Waals interactions and the nonpolar solvation contribution resulting from the burial of the compounds' hydrophobic groups are the basis for favorable binding free energies. The favorable Coulomb interactions within the ligand−protein complexes are opposed by the unfavorable desolvation contribution. The resulting balance of the two contributions is unfavorable to binding in both two systems. The calculations verify the experimental expectation from the viewpoint of energy. Comparing **d26**- with **d25**-bound complexes, it shows that the sum of electrostatic energy including electrostatic interaction and polar contribution to solvation, is similar in both system (22.48 kcal/mol for **d26** and 20.17 kcal/mol for **d25**). Whereas, the sum of van der Waals interaction and the cavity energy of nonpolar solvation contribution of the **d26**-bound is 19.58 kcal/mol less than that of the **d25**-bound, and the difference can partly explain why the conformational change of the **d25**-bound at binding pocket led to its reduced binding affinity.

Free Energy Decomposition. In order to gain further insight into ligand−protein interaction, binding free energy was decomposed to ligand−residue pairs using the MM/GBSA approach. The energy contribution difference of each residue to the **d25**- and **d26**-bound systems are shown in panel (a) of Figure 9. The energy contributions of certain structurally important residues for both complexes are listed in Table S3 of the Supporting Information.

It is shown that almost all residues energetically contribute more for the binding of compound **26** than that of compound **25**, except for residues Ile463, Glu533, Gly534, and Phe583. Comparing **d26** with **d25**, special attention has been paid to several residues with relatively large differences in the contributions to

Table 2. Hydrogen Bonds Analysis from MD[a]

H-bond	donor	acceptor	distance (Å)[b]	occupancy (%)[c]
26-[V600E]B-RAF kinase	ligand N4···H13	Glu501 OE2	2.874	98.4
	Cys532 N···H	Ligand N2	3.05	92.4
	Asp594 N···H	Ligand O2	3.105	83.85
	ligand N3···H12	Cys532 O	2.982	73.95
water-directed	WAT H	Glu501 OE2	2.783	162.05
	WAT H	Ligand O2	3.093	68.25
	WAT H	Asp594 O	2.862	47.2
25-[V600E]B-RAF kinase	ligand N1···H10	Cys532 O	2.799	99.97
	Gly534 N···H	Ligand O3	3.144	66.28
	ligand N4···H13	Thr529 OG1	3.254	8.24
water-directed	WAT H	Glu501 OE2	2.798	38.30
	Asp594 N···H	WAT O	3.088	19.12
	WAT H	Ligand O3	2.834	8.69

[a] The listed donor and acceptor pairs satisfy the criteria for the hydrogen bond over 8.0% of the time during the 10 ns of simulation. [b] The average distance between hydrogen acceptor atom and hydrogen donor atom in the investigated time period. [c] Occupancy is in unit of percentage of the investigated time period.
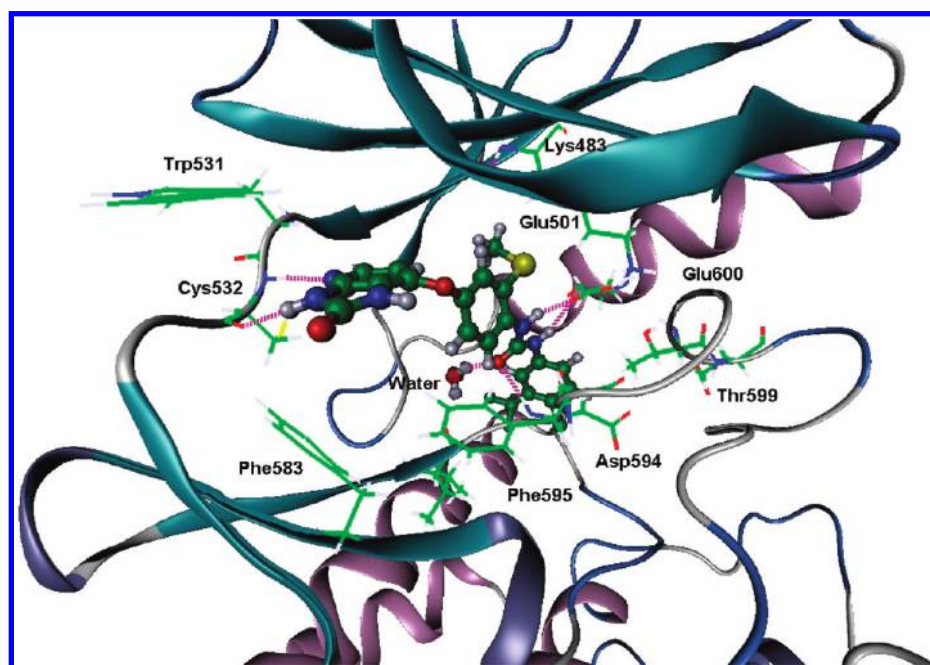

Figure 8. Average conformation of [V600E]B-RAF kinase in a complex with compound **26** during 10 ns of simulation.

binding free energies, such as Val504, Leu505, Leu514, Leu567, and Gly593. It is interesting that all those important residues are hydrophobic, involved in the lipophilic pocket by Phe595 of DFG-out loop, which can form strong van der Waals interactions with the inhibitors. Moreover, the residues with more favorable contributions to the binding process of the **26**-bound [V600E]B-RAF kinase system are residues Glu501, Trp531, Cys532, Asp594, and Phe595, which are functionally important residues for binding. It is observed that their contribution to the binding free energy is more than −10 kcal/mol. To represent the results more intuitively, we plotted the energy contributions of key residues in the active site to the two systems (Figure 9b, c). From

panel (b) of Figure 9, it is shown that the residues Glu501, Trp531, Cys532, Asp594, and Phe595, providing dominant stabilizing forces for the binding process, are mainly responsible for the difference. From panel (c) of Figure 9, it is shown that most residues are in disfavor with the binding for compound **25**, participating in the contribution of total electrostatic energy, while they are slightly unfavorable to that for compound **26**. Especially, the conserved Glu501 and Asp594 involved in the movement of the DFG loop, which can form a bridging H-bond network with compound **26** rather than **25**, that contribute more favorably and less unfavorably to compound **26** than to **25**. From these results, we can conclude that hydrophobic

Table 3. Binding Free Energy Calculations for the d25- and d26-Bound ^{V600E}B-RAF Kinase systems^a

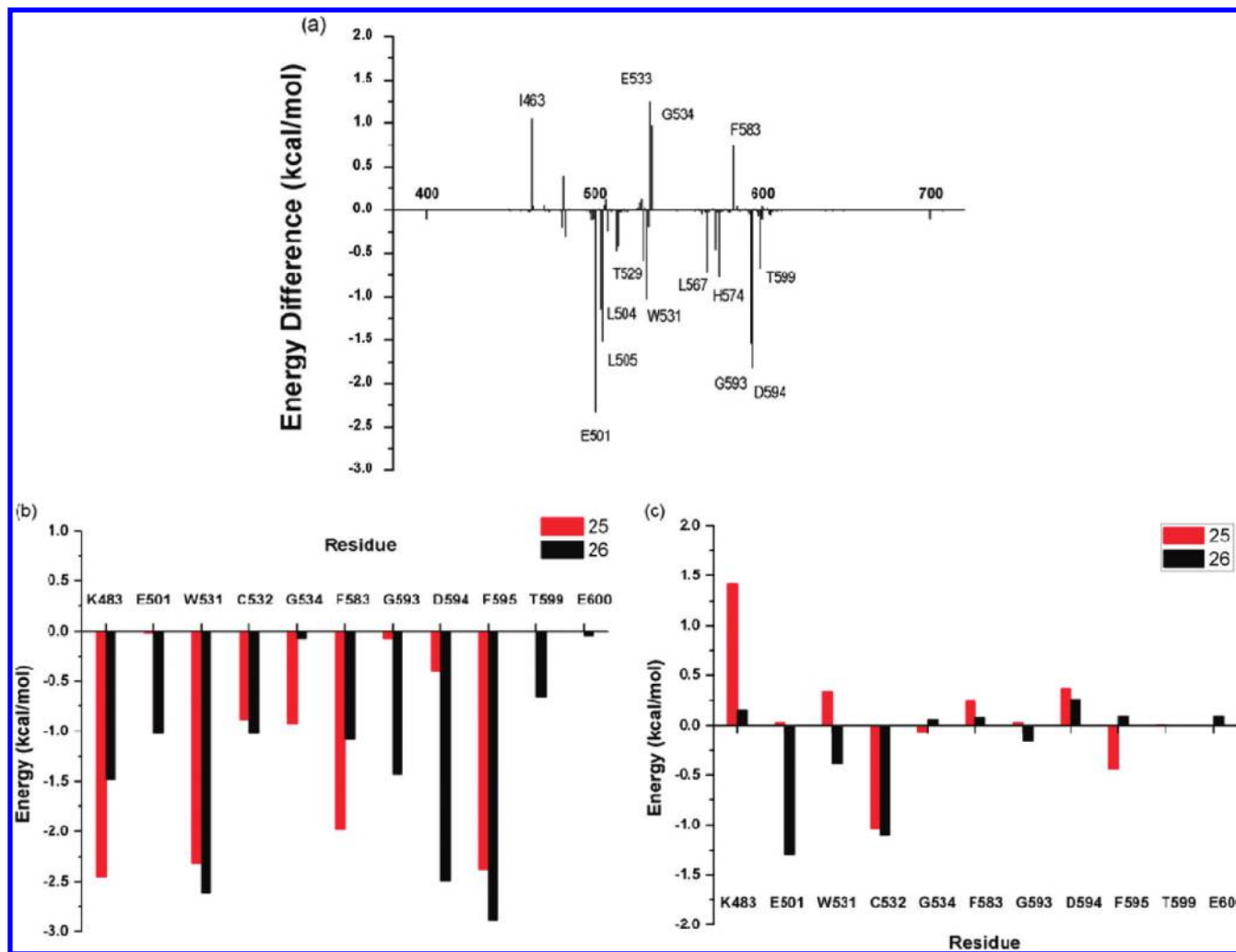|	ΔG_{ele}	ΔG_{vdw}	$\Delta G_{ele,sol}$	$\Delta G_{nonpol,sol}$	ΔG_{MM}	ΔG_{sol}	ΔTS	ΔG_{bind}	$\Delta G_{bind,exp}$
d26	−38.17	−62.77	60.65	−7.78	−100.94	52.87	−26.04	−22.04	−12.35
d25	−18.53	−45.29	38.70	−5.68	−63.82	33.02	−20.11	−10.69	−6.16

^{a} All energies are in kcal/mol.

Figure 9. (a) Energy difference of each residue contribution to the binding of compounds **25** and **26** for ^{V600E}B-RAF kinase. Comparison of the interactions between compounds **25**- and **26**-bound systems for key residues in the active site: (b) VDW and nonpolar solvation energy (ΔG_{vdw} + $\Delta G_{nonpol,sol}$) and (c) electrostatic and polar solvation energy (ΔG_{ele} + $\Delta G_{ele,sol}$).

interactions play an important role in the binding affinity with compound **26** over compound **25**. The formation of a hydrogen bond between compound **26** and the residues Glu501 and Asp594 is favorable to its binding by stabilizing the DFG-out conformation.

4. CONCLUSIONS

In this study, a combined computational approach was applied to gain insight into the structural basis and inhibition mechanism for a series of ^{V600E}B-RAF kinase inhibitors. We obtained several possible binding poses and an accurate ranking of binding affinities for pyridoimidazolone inhibitors using QPLD and GBSA-rescoring. This method reproduced the crystal structure precisely, and the docked results are consistent with the results

from other studies. The molecular dynamics simulation and MM/PBSA calculations confirmed the reasonable binding mode of **d25**- and **d26**-bound complexes and the key interaction features. The calculated binding free energies were in good agreement with the experimental values. The decomposition of binding free energy into each interaction type indicated the van der Waals interactions provided the substantial driving force for the binding process, while energy decomposition to each residue revealed the most favorable contributions came from Glu501, Trp531, Cys532, Gly593, and Asp594. The pivotal hydrogen bond interactions with Glu501 and Asp594 could help stabilize the DFG-out conformation. The results showed the strong H-bond interaction with Glu501, Asp594, and Cys532, and van der Waals interaction with residues in the hydrophobic pocket primarily resulted in the difference for binding and activity

between the two compounds. In addition, a water-mediated H-bond involved in the interaction between Asp594 and compound 26 was observed stably from the MD simulation. The structure-based 3D-QSAR models provided a further structural analysis and modifiable information for understanding the SARs of these inhibitors. The important hydrophobic property of the 3-substitution of the B-ring was required to be Type II inhibitors. The five substitutable positions of the C-ring could be further modified. These results obtained from the computational approach will be helpful for the rational design of novel Type II ^{V600E}B-RAF kinase inhibitors.

■ ASSOCIATED CONTENT

ⓢ **Supporting Information.** Chemical structures of all molecules (Tables S1 and S4); experimental and the predicted pIC_{50} values, docking scores, and MM-GBSA rescores for the training set, test set and external test set (Tables S2 and S5); energy contributions of certain structurally important residues for both complexes (Table S3); structure of the template molecule (compound **26**) aligned in the ABA models (Figure S1); binding mode between ^{V600E}B-RAF kinase and compounds **E1** and **E7** at the active site (Figure S2); and plots of predicted versus observed pIC_{50} values for the external test compounds based on DBA CoMFA and CoMSIA models (Figure S3). This material is available free of charge via the Internet at http://pubs.acs.org.

■ AUTHOR INFORMATION

Corresponding Author
*Tel.: +86-931-891-2578; fax: +86-931-891-2582; e-mail: xjyao@lzu.edu.cn.

■ ACKNOWLEDGMENT

■ REFERENCES

(1) Leicht, D. T.; Balan, V.; Kaplun, A.; Singh-Gupta, V.; Kaplun, L.; Dobson, M.; Tzivion, G. Raf kinases: Function, regulation and role in human cancer. *Biochim. Biophys. Acta* **2007**, *1773*, 1196–1212.

(2) Davies, H.; Bignell, G. R.; Cox, C.; Stephens, P.; Edkins, S.; Clegg, S.; Teague, J.; Woffendin, H.; Garnett, M. J.; Bottomley, W.; Davis, N.; Dicks, E.; Ewing, R.; Floyd, Y.; Gray, K.; Hall, S.; Hawes, R.; Hughes, J.; Kosmidou, V.; Menzies, A.; Mould, C.; Parker, A.; Stevens, C.; Watt, S.; Hooper, S.; Wilson, R.; Jayatilake, H.; Gusterson, B. A.; Cooper, C.; Shipley, J.; Hargrave, D.; Pritchard-Jones, K.; Maitland, N.; Chenevix-Trench, G.; Riggins, G. J.; Bigner, D. D.; Palmieri, G.; Cossu, A.; Flanagan, A.; Nicholson, A.; Ho, J. W.; Leung, S. Y.; Yuen, S. T.; Weber, B. L.; Seigler, H. F.; Darrow, T. L.; Paterson, H.; Marais, R.; Marshall, C. J.; Wooster, R.; Stratton, M. R.; Futreal, P. A. Mutations of the BRAF gene in human cancer. *Nature* **2002**, *417*, 949–954.

(3) Ikenoue, T.; Hikiba, Y.; Kanai, F.; Tanaka, Y.; Imamura, J.; Imamura, T.; Ohta, M.; Ijichi, H.; Tateishi, K.; Kawakami, T.; Aragaki, J.; Matsumura, M.; Kawabe, T.; Omata, M. Functional analysis of mutations within the kinase activation segment of B-Raf in human colorectal tumors. *Cancer Res.* **2003**, *63*, 8132–8137.

(4) Wellbrock, C.; Ogilvie, L.; Hedley, D.; Karasarides, M.; Martin, J.; Niculescu-Duvaz, D.; Springer, C. J.; Marais, R. V599EB-RAF is an oncogene in melanocytes. *Cancer Res.* **2004**, *64*, 2338–2342.

(5) Vandrovcova, J.; Lagerstedt-Robinsson, K.; Pahlman, L.; Lindblom, A. Somatic BRAF-V600E mutations in familial colorectal cancer. *Cancer Epidemiol. Biomarkers Prev.* **2006**, *15*, 2270–2273.

(6) Karasarides, M.; Chiloeches, A.; Hayward, R.; Niculescu-Duvaz, D.; Scanlon, I.; Friedlos, F.; Ogilvie, L.; Hedley, D.; Martin, J.; Marshall, C. J.; Springer, C. J.; Marais, R. B-RAF is a therapeutic target in melanoma. *Oncogene* **2004**, *23*, 6292–6298.

(7) Garnett, M. J.; Marais, R. Guilty as charged: B-RAF is a human oncogene. *Cancer Cell* **2004**, *6*, 313–319.

(8) Madhunapantula, S. V.; Robertson, G. P. Is B-Raf a good therapeutic target for melanoma and other malignancies? *Cancer Res* **2008**, *68*, 5–8.

(9) Smith, R. A.; Dumas, J.; Adnane, L.; Wilhelm, S. M. Recent advances in the research and development of RAF kinase inhibitors. *Curr. Top Med. Chem.* **2006**, *6*, 1071–1089.

(10) Li, N.; Batt, D.; Warmuth, M. B-Raf kinase inhibitors for cancer treatment. *Curr. Opin. Investig. Drugs* **2007**, *8*, 452–456.

(11) Ramurthy, S.; Subramanian, S.; Aikawa, M.; Amiri, P.; Costales, A.; Dove, J.; Fong, S.; Jansen, J. M.; Levine, B.; Ma, S.; McBride, C. M.; Michaelian, J.; Pick, T.; Poon, D. J.; Girish, S.; Shafer, C. M.; Stuart, D.; Sung, L.; Renhowe, P. A. Design and synthesis of orally bioavailable benzimidazoles as Raf kinase inhibitors. *J. Med. Chem.* **2008**, *51*, 7049–7052.

(12) Sala, E.; Mologni, L.; Truffa, S.; Gaetano, C.; Bollag, G. E.; Gambacorti-Passerini, C. BRAF silencing by short hairpin RNA or chemical blockade by PLX4032 leads to different responses in melanoma and thyroid carcinoma cells. *Mol. Cancer Res.* **2008**, *6*, 751–759.

(13) Li, H. F.; Chen, Y.; Rao, S. S.; Chen, X. M.; Liu, H. C.; Qin, J. H.; Tang, W. F.; Yue, W.; Zhou, X.; Lu, T. Recent advances in the research and development of B-Raf inhibitors. *Curr. Med. Chem.* **2010**, *17*, 1618–1634.

(14) Luo, C.; Xie, P.; Marmorstein, R. Identification of BRAF inhibitors through in silico screening. *J. Med. Chem.* **2008**, *51*, 6121–6127.

(15) Fratev, F.; Osk Jonsdottir, S.; Mihaylova, E.; Pajeva, I. Molecular basis of inactive B-RAF(WT) and B-RAF(V600E) ligand inhibition, selectivity, and conformational Stability: An in silico study. *Mol. Pharmaceutics* **2009**, *6*, 144–157.

(16) Fratev, F. F.; Jonsdottir, S. O. An in silico study of the molecular basis of B-RAF activation and conformational stability. *BMC Struct. Biol.* **2009**, *9*, 47.

(17) Fratev, F.; Jonsdottir, S. O. The phosphorylation specificity of B-RAF WT, B-RAF D594V, B-RAF V600E and B-RAF K601E kinases: An in silico study. *J. Mol. Graph. Model.* **2010**, *28*, 598–603.

(18) Alzate-Morales, J. H.; Vergara-Jaque, A.; Caballero, J. Computational study on the interaction of N1 substituted pyrazole derivatives with B-raf kinase: An unusual water wire hydrogen-bond network and novel interactions at the entrance of the active site. *J. Chem. Inf. Model* **2010**, *50*, 1101–1112.

(19) Niculescu-Duvaz, D.; Gaulon, C.; Dijkstra, H. P.; Niculescu-Duvaz, I.; Zambon, A.; Ménard, D.; Suijkerbuijk, B. M. J. M.; Nourry, A.; Davies, L.; Manne, H.; Friedlos, F.; Ogilvie, L.; Hedley, D.; Whittaker, S.; Kirk, R.; Gill, A.; Taylor, R. D.; Raynaud, F. I.; Moreno-Farre, J.; Marais, R.; Springer, C. J. Pyridoimidazolones as novel potent inhibitors of v-Raf murine sarcoma viral oncogene homologue B1 (BRAF). *J. Med. Chem.* **2009**, *52*, 2255–2264.

(20) Ménard, D.; Niculescu-Duvaz, I.; Dijkstra, H. P.; Niculescu-Duvaz, D.; Suijkerbuijk, B. M. J. M.; Zambon, A.; Nourry, A.; Roman, E.; Davies, L.; Manne, H. A.; Friedlos, F.; Kirk, R.; Whittaker, S.; Gill, A.; Taylor, R. D.; Marais, R.; Springer, C. J. Novel potent BRAF inhibitors: Toward 1 nM compounds through optimization of the central phenyl ring. *J. Med. Chem.* **2009**, *52*, 3881–3891.

(21) Niculescu-Duvaz, I.; Roman, E.; Whittaker, S. R.; Friedlos, F.; Kirk, R.; Scanlon, I. J.; Davies, L. C.; Niculescu-Duvaz, D.; Marais, R.; Springer, C. J. Novel inhibitors of the v-raf murine sarcoma viral oncogene homologue B1 (BRAF) based on a 2,6-disubstituted pyrazine scaffold. *J. Med. Chem.* **2008**, *51*, 3261–3274.

691

dx.doi.org/10.1021/ci100427j |*J. Chem. Inf. Model.* 2011, 51, 680–692

(22) Zambon, A.; Menard, D.; Suijkerbuijk, B. M. J. M.; Niculescu-Duvaz, I.; Whittaker, S.; Niculescu-Duvaz, D.; Nourry, A.; Davies, L.; Manne, H. A.; Lopes, F.; Preece, N.; Hedley, D.; Ogilvie, L. M.; Kirk, R.; Marais, R.; Springer, C. J. Novel hinge binder improves activity and pharmacokinetic properties of BRAF inhibitors. *J. Med. Chem.* **2010**, *53*, 5639–5655.

(23) Suijkerbuijk, B. M.; Niculescu-Duvaz, I.; Gaulon, C.; Dijkstra, H. P.; Niculescu-Duvaz, D.; Menard, D.; Zambon, A.; Nourry, A.; Davies, L.; Manne, H. A.; Friedlos, F.; Ogilvie, L. M.; Hedley, D.; Lopes, F.; Preece, N. P.; Moreno-Farre, J.; Raynaud, F. I.; Kirk, R.; Whittaker, S.; Marais, R.; Springer, C. J. Development of novel, highly potent inhibitors of V-RAF murine sarcoma viral oncogene homologue B1 (BRAF): Increasing cellular potency through optimization of a distal heteroaromatic group. *J. Med. Chem.* **2010**, *53*, 2741–2756.

(24) Nourry, A.; Zambon, A.; Davies, L.; Niculescu-Duvaz, I.; Dijkstra, H. P.; Menard, D.; Gaulon, C.; Niculescu-Duvaz, D.; Suijker-buijk, B. M.; Friedlos, F.; Manne, H. A.; Kirk, R.; Whittaker, S.; Marais, R.; Springer, C. J. BRAF inhibitors based on an imidazo[4,5]pyridin-2-one scaffold and a meta substituted middle ring. *J. Med. Chem.* **2010**, *53*, 1964–1978.

(25) *Maestro*, version 9.0; Schrödinger, LLC: New York, 2009.

(26) *MacroModel*, version 9.7; Schrödinger, LLC: New York, 2009.

(27) Smith, A. L.; DeMorin, F. F.; Paras, N. A.; Huang, Q.; Petkus, J. K.; Doherty, E. M.; Nixey, T.; Kim, J. L.; Whittington, D. A.; Epstein, L. F.; Lee, M. R.; Rose, M. J.; Babij, C.; Fernando, M.; Hess, K.; Le, Q.; Beltran, P.; Carnahan, J. Selective inhibitors of the mutant B-Raf pathway: Discovery of a potent and orally bioavailable aminoisoquino-line. *J. Med. Chem.* **2009**, *52*, 6189–6192.

(28) *Discovery Studio*, version 2.5.5; Accelrys, Inc.: San Diego, CA, 2010.

(29) *Impact*, version 5.0; Schrödinger, LLC: New York, 2005.

(30) *QM-Polarized Ligand Docking Protocol*; *Glide*, version 5.5; *Jaguar*, version 7.6; *QSite*, version 5.5; Schrödinger, LLC: New York, 2009.

(31) *Prime*, version 2.0; Schrödinger, LLC: New York, 2008.

(32) Lyne, P. D.; Lamb, M. L.; Saeh, J. C. Accurate prediction of the relative potencies of members of a series of kinase inhibitors using molecular docking and MM-GBSA scoring. *J. Med. Chem.* **2006**, *49*, 4805–4808.

(33) Guimaraes, C. R.; Cardozo, M. MM-GB/SA rescoring of docking poses in structure-based lead optimization. *J. Chem. Inf. Model* **2008**, *48*, 958–970.

(34) *Sybyl*, version 6.9; Tripos Associates: St. Louis, MO, 1999.

(35) Cramer, R. D.; Patterson, D. E.; Bunce, J. D. Comparative molecular field analysis (CoMFA). 1. Effect of shape on binding of steroids to carrier proteins. *J. Am. Chem. Soc.* **1988**, *110*, 5959–5967.

(36) Klebe, G.; Abraham, U.; Mietzner, T. Molecular similarity indices in a comparative analysis (CoMSIA) of drug molecules to correlate and predict their biological activity. *J. Med. Chem.* **1994**, *37*, 4130–4146.

(37) Du, J.; Qin, J.; Liu, H.; Yao, X. 3D-QSAR and molecular docking studies of selective agonists for the thyroid hormone receptor beta. *J. Mol. Graphics Modell.* **2008**, *27*, 95–104.

(38) Qin, J.; Liu, H.; Li, J.; Ren, Y.; Yao, X.; Liu, M. 3D-QSAR studies on the inhibitors of AP-1 and NF-kappaB mediated transcriptional activation. *Eur. J. Med. Chem.* **2009**, *44*, 2888–2895.

(39) Wold, S. Cross validatory estimation of the number of compo-nents in factor and principal components models. *Technometrics* **1978**, *20*, 397–405.

(40) Ståhle, L.; Wold, S. Partial least squares analysis with cross-validation for the two-class problem: A Monte Carlo study. *J. Chemom.* **1987**, *1*, 185–196.

(41) Cramer, R. D., III; Bunce, J. D.; Patterson, D. E.; Frank, I. E. Crossvalidation, bootstrapping, and partial least squares compared with multiple regression in conventional QSAR studies. *Quant. Struct.-Act. Relat.* **1988**, *7*, 18–25.

(42) Kearns, M.; Ron, D. Algorithmic stability and sanity-check bounds for leave-one-out cross-validation. *Neural. Comput.* **1999**, *11*, 1427–1453.

(43) Case, D. A.; Cheatham, T. E., 3rd; Darden, T.; Gohlke, H.; Luo, R.; Merz, K. M., Jr.; Onufriev, A.; Simmerling, C.; Wang, B.; Woods, R. J. The AMBER biomolecular simulation programs. *J. Comput. Chem.* **2005**, *26*, 1668–1688.

(44) Duan, Y.; Wu, C.; Chowdhury, S.; Lee, M. C.; Xiong, G.; Zhang, W.; Yang, R.; Cieplak, P.; Luo, R.; Lee, T.; Caldwell, J.; Wang, J.; Kollman, P. A point-charge force field for molecular mechanics simula-tions of proteins based on condensed-phase quantum mechanical calculations. *J. Comput. Chem.* **2003**, *24*, 1999–2012.

(45) Wang, J.; Wolf, R. M.; Caldwell, J. W.; Kollman, P. A.; Case, D. A. Development and testing of a general AMBER force field. *J. Comput. Chem.* **2004**, *25*, 1157–1174.

(46) Bayly, C. I.; Cieplak, P.; Cornell, W.; Kollman, P. A. A well-behaved electrostatic potential based method using charge restraints for deriving atomic charges: The RESP model. *J. Phys. Chem.* **1993**, *97*, 10269–10280.

(47) Jorgensen, W.; Chandrasekhar, J.; Madura, J.; Impey, R.; Klein, M. Comparison of simple potential functions for simulating liquid water. *J. Chem. Phys.* **1983**, *79*, 926–935.

(48) Essmann, U.; Perera, L.; Berkowitz, M. L.; Darden, T. A smooth particle mesh Ewald method. *J. Chem. Phys.* **1995**, *103*, 8577–9593.

(49) Ryckaert, J.; Ciccotti, G.; Berendsen, H. Numerical integration of the cartesian equations of motion of a system with constraints: Molecular dynamics of *n*-alkanes. *J. Comput. Phys.* **1977**, *23*, 327–341.

(50) Gohlke, H.; Kiel, C.; Case, D. A. Insights into protein−protein binding by binding free energy calculation and free energy decomposi-tion for the Ras-Raf and Ras-RalGDS complexes. *J. Mol. Biol.* **2003**, *330*, 891–913.

(51) Vickie, T.; David, A. C. Theory and applications of the general-ized born solvation model in macromolecular simulations. *Biopolymers* **2000**, *56*, 275–291.

(52) Mathew, C. L.; Yong, D. Distinguish protein decoys by using a scoring function based on a new AMBER force field, short molecular dynamics simulations, and the generalized born solvent model. *Proteins* **2004**, *55*, 620–634.

(53) Hou, T.; Xu, Z.; Zhang, W.; McLaughlin, W. A.; Case, D. A.; Xu, Y.; Wang, W. Characterization of domain−peptide interaction interface. *Mol. Cell. Proteomics* **2009**, *8*, 639–649.

(54) Hou, T.; Zhang, W.; Case, D. A.; Wang, W. Characterization of domain−peptide interaction interface: A case study on the amphiphy-sin-1 SH3 domain. *J. Mol. Biol.* **2008**, *376*, 1201–1214.

(55) Wang, J.; Morin, P.; Wang, W.; Kollman, P. A. Use of MM-PBSA in reproducing the binding free energies to HIV-1 RT of TIBO derivatives and predicting the binding mode to HIV-1 RT of efavirenz by docking and MM-PBSA. *J. Am. Chem. Soc.* **2001**, *123*, 5221–5230.